Sustainable Energy Technologies and Assessments 88 (2026) 104949

Contents lists available at ScienceDirect

Sustainable Energy Technologies and Assessments

journal homepage: www.elsevier.com/locate/seta

Exploring optimized solutions for wind and solar power deployment in a case study for the Canary Islands

Sonia Jerez [a,*], Judit Carrillo [b], Albano González [b], Juan Pedro Díaz [b], Francisco Javier Expósito [b], Juan Carlos Pérez Darias [b]

[a] Department of Physics, University of Murcia, Spain
[b] GOTA Group, Universidad de La Laguna, Spain

ABSTRACT

Solar and wind power are key pillars in the transition toward decarbonized electricity systems, but their integration is challenged by weather-driven intermittency. To address this, the CLIMAX tool was developed to support actionable strategies for deploying wind and solar photovoltaic (PV) facilities that reduce production volatility. In this case study, CLIMAX is applied to the Canary Islands, an insular region with diverse climatic conditions, to generate optimized deployment scenarios. The objective is to minimize residual demand (net electricity demand minus renewable generation) by leveraging the spatio-temporal complementarity of wind and solar resources. Results show that optimized strategies can improve system stability by up to 20 percentage points relative to current deployment patterns. These gains are achieved through a balanced approach that combines (i) adjustment of the wind-to-solar ratio in the mix, and (ii) spatial redistribution of facilities to prioritize complementarity rather than mere productivity. As a trade-off, optimized configurations often involve lower capacity factors, since site selection considers joint performance rather than isolated potential. The study also assesses the role of urban rooftop PV systems, demonstrating that ambitious coverage thresholds could transform underused urban surfaces into valuable energy assets — an insight with clear implications for integrated planning and renewable energy policy.

Introduction

Advancing the transition toward autonomous, low-carbon energy systems is an urgent priority, both to (1) meet zero emissions targets required to mitigate climate change [1], and (2) enhance energy security in an increasingly complex and challenging geopolitical context[2,3]. Wind and solar power are expected to lead this transition, alongside the electrification of energy systems[4]. Although these mature technologies already represent a substantial share of energy generation worldwide, a massive deployment of new facilities is still forthcoming [5]. The way this expansion unfolds is critical, as well-informed, well-planned deployment strategies can significantly improve system resilience[6] and help reduce undesirable fluctuations in electricity generation from inherently variable sources such as wind and solar radiation [7–9], and thereby mismatches between energy production and demand.

The climate science community has been urged to increase efforts to improve the accuracy of predictions and simulations of variables that, in this context, gain particular relevance: wind speed at typical hub heights and downward surface solar radiation [10,11]. Accordingly, advances are also being made in understanding the behavior and long-term evolution of these resources by identifying their key drivers, including large-scale climate variability modes[12]and external forcing agents such as aerosols[13]. This growing body of knowledge is then applied to provide actionable insights for energy planning, with one key area of interest being the spatio-temporal complementarity between wind and solar resources[14]. Such complementarity enables for a more stable energy supply: when one resource underperforms, the other may compensate (temporal complementarity), or energy production can be balanced across neighboring areas (spatial complementarity). To leverage and operationalize these concepts, the free-access, open-source CLIMAX tool[15]was recently developed. Taking advantage of such a complementarity, CLIMAX identifies *ad-hoc* optimal spatial distributions and shares of wind and solar photovoltaic (PV) facilities within a selected region.

In this study, we apply CLIMAX to explore optimized deployment strategies for wind and solar power in the Canary Islands, a geographically complex and isolated archipelago located in the North Atlantic Ocean near the African coast. This case study offers significant potential for optimization because of the islands' diverse climate. Furthermore, as an insular system, energy self-sufficiency is essential. Hence, the Canary Islands exemplify many of the challenges (and opportunities) faced by other isolated regions in transitioning to renewable energy. In addition, we assess the role of urban areas in supporting this transition, as rooftop PV panels play a crucial role in minimizing the environmental impact of

* Corresponding author.
E-mail address: sonia.jerez@um.es (S. Jerez).

https://doi.org/10.1016/j.seta.2026.104949
Received 3 July 2025; Received in revised form 24 November 2025; Accepted 23 March 2026
Available online 27 March 2026

large-scale solar power deployment by utilizing already-built surfaces instead of requiring additional land use transformation for ground-based installations, an especially relevant advantage given limited land availability.

Domain and data

This case study focuses on the Canary Islands archipelago, which comprises eight islands (Fig. 1a). Although their respective electric grids are not interconnected except for the eastern islands, namely Fuerteventura, Lanzarote, and La Graciosa, here we consider that the whole system of islands is ideally interconnected (which enhances optimization of decarbonized scenarios, [16], disregarding transmission losses. Certainly, the interconnection between La Gomera and Tenerife is currently under construction, but others remain limited by technical constraints mainly related to the steep bathymetry in the region. This is, therefore, a strictly academic exercise aimed at illustrating the full potential of the method for optimized solutions. The data required by this

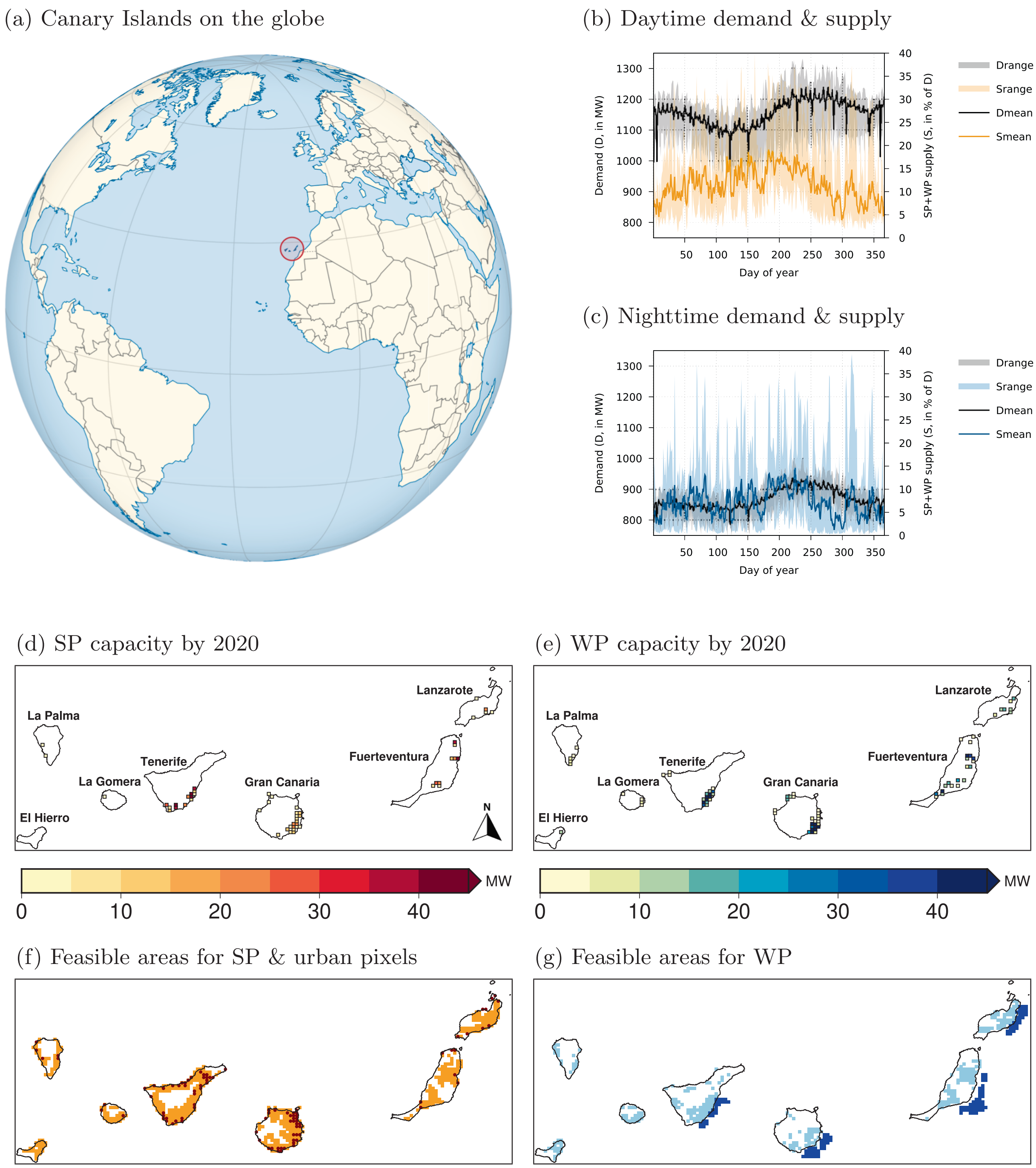

Fig. 1. Domain. Panel (a): Location of the Canary Islands archipelago on the globe. Panels (b) and (c): Daymeans of daytime and nighttime SP + WP supply (yellow and blue, respectively) and electricity demand (grey) in the whole archipelago. Thick lines are daily multi-year means, thus depicting mean annual cycles. Shadows show the maximum deviation from the mean of the individual daily records in the series, which span from 2014 to 2019. Panels (d) and (e): Operative or programmed capacity of solar photovoltaic (SP) and wind power (WP), respectively, by the year 2020 aggregated per grid cell (units: MW), with the name of each island indicated in panel (d). Panels (f) and (g): Feasible areas for the deployment of SP (orange) and WP (light blue for onshore and dark blue for offshore), respectively, with the grid cells comprising urban areas highlighted in red in panel (f).

research are described below.

Electricity demand records (from all the islands comprising the Canarian system) with hourly resolution for the period 2014–2019, provided by the transmission agent and operator of the Spanish electricity system (*Red Eléctrica de España*, www.ree.es, last accessed on June 20, 2025), were used in this study to try fitting simulated electricity production series to demand. With a merely illustrative purpose, Fig. 1b, c provides a picture of the mean demand along the year, for both day- and nighttime, and its interannual variations, together with the actual wind-plus-solar power supply (also retrieved from the same source with the same hourly resolution and for the same period).

Weather variables were used to estimate wind and solar power (WP and SP, respectively) capacity factors (*CF*), specifically, downward surface solar radiation (*rsds*) and wind speed (*ws*) at two vertical levels, 100 and 150 m height. These were obtained from a high spatio-temporal resolution regional climate simulation performed with the WRF model [17]to downscale the ERA5 reanalysis[18]. This simulation provides two-hourly data data on a spatial grid with 3 km horizontal resolution for the period 2014–2019. The WRF configuration, including the three nested domains used (with 27, 9, and 3 km of spatial resolution,

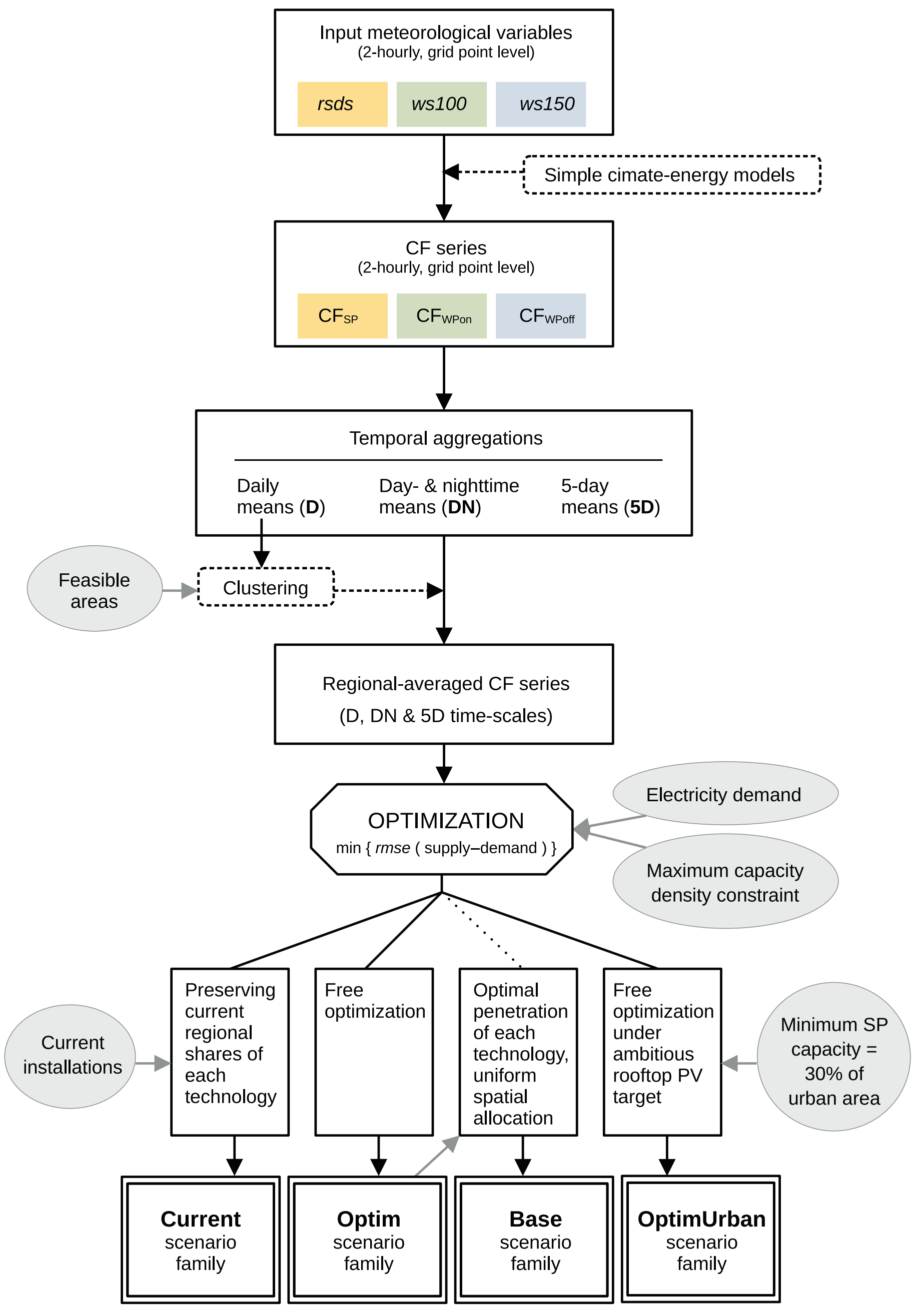

Fig. 2. Workflow. Schematic diagram of the methodological steps followed in this study (described in Section 3). Weather data (solar radiation and wind speed at two heights) are first converted into 2-hourly grid-point level capacity factor (CF) series for solar photovoltaic (SP), onshore wind (WPon), and offshore wind (WPoff) power, using simple climate-energy models. These CF series are then aggregated in time (daily means, day- and nighttime means, and 5-day means) and in space (into regions with similar CF temporal variability). The resulting regional mean CF series, together with electricity demand and technical constraints (e.g., capacity density limits, minimum urban solar contribution), feed the CLIMAX optimization framework, which produces four families of deployment scenarios: (i) Current (based on existing regional shares of each technology), (ii) Optim (fully optimized), (iii) Base (homogeneous distribution across regions preserving optimized total shares of each technology), and (iv) OptimUrban (optimized with a minimum urban SP constraint).

respectively) and the selection of physical parameterizations used for those processes that are not explicitly resolved, was adopted from previous works in which the model performance has been compared with observations of different variables such as wind, solar radiation, temperature, precipitation, etc. [19–22]. Specifically, the selected physics schemes were the WRF double-moment 6-class for microphysics [23], the Yonsei University planetary boundary layer scheme[24], the Noah land surface model[25], and the Community Atmosphere Model version 3 scheme[26]for both longwave and shortwave radiation. The Kain–-Fritsch scheme[27]was selected for cumulus parameterization, being switched off in the innermost domain since the spatial resolution is sufficiently high to perform a convection-permitting simulation. Fifty unevenly distributed vertical levels were used, with higher concentration in the lower part of the atmosphere.

Finally, WP and SP facilities that were either operative or planned (formally approved or under construction) by the end of 2020, as reported by DGIEGC [28,29], were aggregated per grid cell, using the spatial grid of the WRF simulation (Fig. 1d,e), to construct current deployment scenarios (see next Section). To construct the optimized deployment scenarios, only those onshore grid cells identified in MTERD [30] as suitable or profitable for allocating WP or SP installations were considered (Fig. 1f,g). The areas for offshore wind energy were obtained from the Spanish Government's Maritime Space Management Plans (POEM), which establish areas of high potential and priority use for the development of offshore wind energy in the different Spanish marine territories[30]. The grid points densely covered by urban areas were obtained from the database provided by GRAFCAN [31].

Methodology

This Section describes the methodological steps followed in this study, summarized in the flowchart of Fig. 2.

Capacity factors

We follow Jerez & Trigo [10] to construct WP and SP *CF* series from weather variables. Hence, SP *CF* is estimated from the *rsds* values (in W m^{-2}) using Equation (1), where G_{STC} refers to the incoming surface short-wave radiation at standard test conditions (1000 W m^{-2}) and P_R is the performance ratio accounting for system losses (typically 0.75, dimensionless).

$$CF = \frac{rsds}{G_{STC}} P_R \tag{1}$$

For WP, a typical wind power curve (Equation (2) is used, defining cut-in, rated, and cut-off speeds (w_I, w_R, and w_O, respectively) of 4, 12, and 25 m s^{-1} to estimate *CF* from *ws* values. WP *CF* was computed at two heights, 100 and 150 m, assuming different hub heights for on-shore and off-shore locations, respectively. *ws* at 100 m (onshore) and 150 m (offshore) was vertically interpolated between the two closest WRF model levels using the standard utilities provided by the wrf-python package (https://wrf-python.readthedocs.io), which accounts for WRF's hybrid terrain-following vertical coordinate system. Although a high density of vertical levels is considered in the lowest part of the atmosphere, they rarely coincide exactly with heights of 100 and 150 m above the surface. The interpolation is linear and ignores air-density effects, as their impact over the 100–150 m layer is negligible compared to that of wind-speed variability.

$$CF = \begin{cases} 0, & \text{if} \quad ws < w_I \\ \dfrac{ws^3 - w_I{}^3}{w_R{}^3 - w_I{}^3}, & \text{if} \quad w_I \le ws < w_R \\ 1, & \text{if} \quad w_R \le ws < w_O \\ 0, & \text{if} \quad ws \ge w_O \end{cases} \tag{2}$$

Regions

The grid points within the feasible areas for SP and WP deployments (Fig. 1f,g) are clustered into regions showing similar temporal variability of the daily anomalies (with respect to the mean daily annual cycle) of the *CF* series of each technology, respectively, as in Jerez et al. [15]. As explained there (and elsewhere), once these regions are defined, it permits the use of the regional mean *CF* series instead of those from the single grid points. Hence, this non-necessary but recommended step pursues, in the context of this work, two objectives. First, reducing the degrees of freedom for the optimization exercise — from thousands (the number of grid points) to tens (the number of regions). Second, enhancing the flexibility and feasibility of the resulting solutions, which will be in the form of regional targets (easier to accommodate than if specified at the grid point level).

The clustering method consists of three steps. It first performs a Principal Component Analysis (PCA) on the input series. Based on the PCA results, a subset of the resulting Empirical Orthogonal Functions (EOFs) must be retained. This decision is up to the user and was made here given their explained variance (Supplementary Fig. S1, left): 21 for the SP series, 15 for the WP onshore series, and 4 for the WP offshore series, with cumulative explained variances exceeding 80, 90, and 95%, respectively. Then, Ward's hierarchical method [32] is applied, which computes Ward's distances defined in the EOFs space (Euclidean distance between the retained eigenvectors from the PCA) as a function of the number of clusters. Based on this analysis, the user must decide the number of clusters to be obtained. Here, 25, 18, and 8 for the SP, WP onshore, and WP offshore, respectively. This decision was guided by a visual inspection of the Ward-distance curves (Supplementary Fig. S1, right), supported by objective criteria including the use of a piecewise linear regression, the L-method [33], which identifies a breakpoint between a steep-slope/high-gain and a low-slope/diminishing-returns linear regime (applied here to the last 25% of the hierarchical merging steps), and the Elbow method[34], which detects the point of maximum deviation from the straight-line trend in the Ward-distance curve. Finally, with the seeds from this first-guess classification, the non-hierarchical k-means clustering algorithm[35]is applied to obtain the final clusters. Details on this methodology can be found in Lorente-Plazas et al. [36].

The final clusters (here, referred to as regions) are depicted in Fig. 3 (left panels). Although alternative region counts could also yield valid configurations and the number of regions can be adapted depending on the study objectives, data availability, or decision-maker needs, this choice effectively captures the windward-leeward pattern which, in combination with the complex orography, plays a dominant role in shaping the climatological characteristics of the Canary Islands. Fig. 3 (right panels) also presents the matrices showing temporal correlations between the regional averaged time series of *CF* daily anomalies. Dark blue colors denote strong positive correlations, implying a lack of complementarity between regions/energies, while light and red colors indicate weak or negative correlations, highlighting the potential complementary among those regions or energy sources, which is most evident when both energies, SP and WP, are combined (Fig. 3f).

Scenarios

We created four families of deployment scenarios. Two of them (Current and Base) will serve as a reference to evaluate the benefits of a fully optimized scenario (Optim). This latter uses the free-access open-source CLIMAX tool[15] to leverage the joint wind-plus-solar production in terms of minimal deviations from the demand by identifying the best spatial distribution and shares of each technology (i.e. how much capacity of each technology should be allocated in each region) under the only restriction of a maximum capacity density of 80, 8, and 15 MW/km^2 for SP, WP onshore, and WP offshore, respectively [37]– although

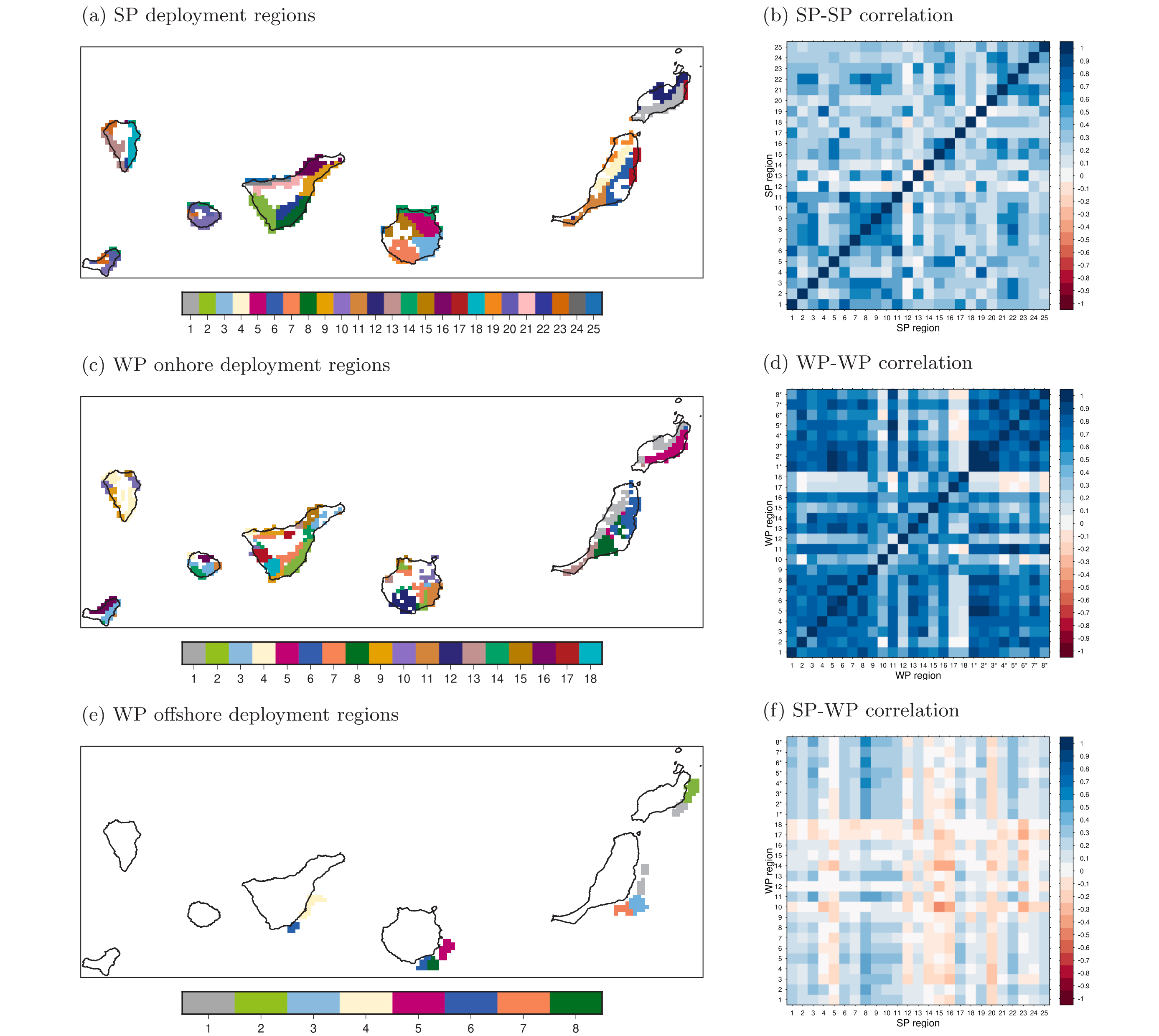

Fig. 3. Regions. On the left-hand side, regions (identified by the color and corresponding number in the color bars), within the feasible areas for facility deployment, with homogeneous temporal variability of the CF daily mean series of (a) solar photovoltaic, (c) onshore wind, and (e) offshore wind power over the corresponding feasibility areas. On the right-hand side, the cross-correlation matrix of the regional-averaged CF daily mean series between regions (panel b for SP and panel d for WP) and between regions and technologies (f). Stars denote offshore regions in panels (d) and (f). Dark blue indicates high positive correlation (low complementarity), while red indicates negative correlation.

these capacity density thresholds ultimately proved to be non-binding, as they were not even close to being reached.

The optimization seeks to minimize the following *rmse* function:

$$\sqrt{\frac{\sum_{n=1}^{NT}(P_n - D_n)^2}{NT}} \tag{3}$$

where NT is the number of time steps in the series, D is the electricity demand, and P is the joint wind-plus-solar production, both in MWh. Thus, P at the n^{th}-time step (P_n) is given by:

$$P_n = \sum_{i=1}^{NR_{SP}} I_i^{SP} CF_{i,n}^{SP} + \sum_{j=1}^{NR_{WPon}} I_j^{WPon} CF_{j,n}^{WPon} + \sum_{k=1}^{NR_{WPoff}} I_k^{WPoff} CF_{k,n}^{WPoff} \tag{4}$$

being NR_{SP}, NR_{WPon}, and NR_{WPoff} the number of regions identified in Section 3.2 for the deployment of SP, WP onshore, and WP offshore, respectively, CF the respective regional averaged capacity factors series, and I the installed capacities of each technology in each region (in MW), the free parameters subject to optimization here.

Three Optim scenarios were developed, each corresponding to a distinct time-interval over which the demand and production series were aggregated (aggregation precedes optimization): OptimD was constructed for fitting daily means series (with one value per day, $NT =$ 6 years of data $\times$ 365 $=$ 2190), OptimDN for day- and nighttime daily mean series (with two values per day, $NT = 2190 \times 2 = 4380$, where daytime means were computed from all records between 10 a.m. and 9p. m., and nighttime means from the remaining hours), and Optim5D for five-day mean series (with one value each five days, $NT = 2190$ / $5 =$ 438). The differentiation between daytime and nighttime values was introduced to account for the absence of solar generation at night and its effects on the simulations. The five-day temporal aggregation was used to study the relative importance of daily variability in modeling the distribution of different types of energies.

Once the I optimal values are determined (see Table S1 in Supplementary Material, which, besides I values, includes a summary of the results for each scenario and aggregation time-scale), the optimal shares (S, in parts per unit) of each energy in each region are straightforwardly calculated as:

$$S_i^{SP} = \frac{I_i^{SP}}{I_{tot}}, \quad S_j^{WPon} = \frac{I_j^{WPon}}{I_{tot}}, \text{ and } \quad S_k^{WPoff} = \frac{I_k^{WPoff}}{I_{tot}} \quad (5, 6, \text{and } 7).$$

where

$$I_{tot} = I_{tot}^{SP} + I_{tot}^{WPon} + I_{tot}^{WPoff} = \sum_{i=1}^{NR_{SP}} I_i^{SP} + \sum_{j=1}^{NR_{WPon}} I_j^{WPon} + \sum_{k=1}^{NR_{WPoff}} I_k^{WPoff} \quad (8)$$

with all I values expressed in MW.

The analysis focuses on S values instead of I values, disregarding the magnitude of I_{tot} due to its likely susceptibility to systematic bias errors in the simulated weather variables and inaccuracies in the CF modeling approaches (Equations (1) and (2), which do not prevent us, however, from trusting the modeled CF variability.

To construct the Current scenarios, the actual value of the factor I_{tot} was disregarded. These scenarios represent the current spatial distribution of facilities (as shown in Fig. 1d,e), using a value of I_{tot} that was optimally scaled so that the modeled production series fit the observed demand as closely as possible. Specifically, Current scenarios were constructed as follows. First, known installations (Fig. 1d,e) were aggregated per region. Second, in Equation (4), each I value was replaced by the corresponding S value multiplied by an "unknown" factor I_{tot}. Equation (3) was then minimized to obtain the optimal value of I_{tot}. This was done three times to construct the CurrentD, CurrentDN, and Current5D scenarios. This way, the Current and Optim scenarios are directly comparable and, from this comparison, the added value of the optimized scenarios, in terms of both the spatial distribution of the facilities and the share/weight given to each energy, can be figured out.

The Base scenarios keep the Optim total shares of each energy (as defined in Equations 9, 10, and 11; note that the sum of the total shares of each energy is, by definition/construction, the unit), but the facilities are supposed to be homogeneously distributed across the feasible areas for each technology. Hence, regional shares in the Base scenarios are just proportional to the size of each region, and the comparison of the Optim and Base scenarios will show up the isolated added value of a smart spatial distribution of the renewable units.

$$S_{tot}^{SP} = \sum_{i=1}^{NR_{SP}} S_i^{SP}, \quad S_{tot}^{WPon} = \sum_{j=1}^{NR_{WPon}} S_j^{WPon}, \text{ and } \quad S_{tot}^{WPoff} = \sum_{k=1}^{NR_{WPoff}} S_k^{WPoff} \quad (9, 10, \text{and } 11).$$

In summary, Optim and Base scenarios maintain the same total share of each technology, differing in the spatial density patterns (spatial distribution) of the facilities (being flat in the Base scenarios), while Current scenarios preserve both the current total shares of each technology and the spatial density patterns of the facilities.

Finally, to assess the potential role and contribution of urban areas in optimized deployment strategies, we developed the OptimUrban scenarios. These scenarios follow the same optimization approach as the Optim ones, but include an additional constraint requiring that at least 30% of the available rooftop area be covered with PV panels. This ambitious assumption (current regulation mandates 7.5%) aims to explore the upper bound of the potential urban solar contribution to large-scale renewable integration when fully leveraged. The minimum rooftop SP capacity in each region was computed by applying the maximum solar capacity density (80 MW/km^2) to 30% of the mapped urban area. This minimum was imposed as a constraint in the optimization, while the remaining capacity (SP or WP) was optimally distributed across regions to minimize residual demand, as in the Optim approach. No distinction was made between rooftop and ground-based PV in terms of capacity factor modeling, which is based on the same regional CF series.

Results

Current scenario

First, the suitability of the current deployment strategy is assessed using the Current scenarios, shown in Fig. 4 (left panels). Preserving both the current total share of each technology (33% SP, 66% WP onshore, and 1% WP offshore) and the existing spatial density patterns of the facilities, the resulting ability to meet demand from SP and WP remains relatively moderate, as illustrated in the right panels of Fig. 4. These panels display the mean annual cycles (thick lines) of the simulated wind-plus-solar supply (expressed as a percentage of demand), along with the corresponding interannual variations (max–min-range, with shadows), for the various time-scales: daily means, daytime and nighttime daily means, and 5-day means. They also provide mean supply values (averaged over the entire period of data) and the root mean squared error between production and demand (*rmse*, computed as in Equation (3), expressed as a percentage of the mean demand. For each row in the figure, optimization was performed with the corresponding time series. Thus, for example, the first row corresponds to the results, for various time aggregations, when the optimization searching for I_{tot} was performed by minimizing the root mean square difference between the simulated energy and the total demand using the daily time series (D). Ideally, a perfect match between wind-plus-solar supply and demand would be represented by a flat thick line at 100% with no shading (*mean* = 100% and *rmse* = 0%).

Far from that optimum, on average, the current scenario would provide a mean supply around 80% of the mean demand, dropping to 75% at nighttime in the CurrentD and CurrentDN scenarios (which are nearly identical), with *rmse* values ranging between 40% and 50%, indicating low system stability and a limited ability to follow consumption patterns. The system fails to ensure a stable supply, similarly in the three analyzed scenarios (CurrentD, CurrentDN, and Current5D). The Current5D scenario achieves a slight improvement in mean production, but only by considering a slightly higher I_{tot} value compared to the other scenarios, which, however, does not lead to a significant reduction in rmse values.

Optimal scenarios

The optimal strategy for matching the daily mean supply and demand series (OptimD scenario, Fig. 5a) relies heavily on SP (86% share), with most facilities concentrated in a few regions, specifically, the southwest of Tenerife, areas in the southwest and north of Gran Canaria, and a large portion of Lanzarote. As a result, this scenario provides mean supply values close to 100% of the mean demand (specifically, 96%; this comes at the cost of doubling the installed capacity compared to the Current scenarios) and reduces the production-demand mismatch (the rmse) to approximately half of the values obtained in the CurrentD scenario both at the daily and 5-day mean time scales (Fig. 5b and 5e). However, it still struggles to meet nighttime demand (Fig. 5d). This limitation would make it necessary to rely on backup energy sources or energy storage systems.

If energy storage requirements do not pose a major constraint for energy planning, the Optim5D scenario (Fig. 5k) could be considered a viable option. By considering longer time intervals, a better match between supply and demand can be achieved, albeit at the cost of increased storage needs. However, in this case, the results show no significant differences between the outcomes from the Optim5D (Fig. 5 m-o) and OptimD (Fig. 5 b-e) scenarios. Both are very similar, exhibiting nearly identical values of total penetration (I_{tot}), technology shares, and spatial distribution of facilities (Fig. 5a *vs.* Fig. 5k).

Conversely, when energy storage capacity is highly constrained, the need to ensure nighttime supply becomes more critical. To address this limitation, the OptimDN scenario was developed (Fig. 5f), in which WP plays a dominant role (40% SP share, 48% WP onshore share, 12% WP

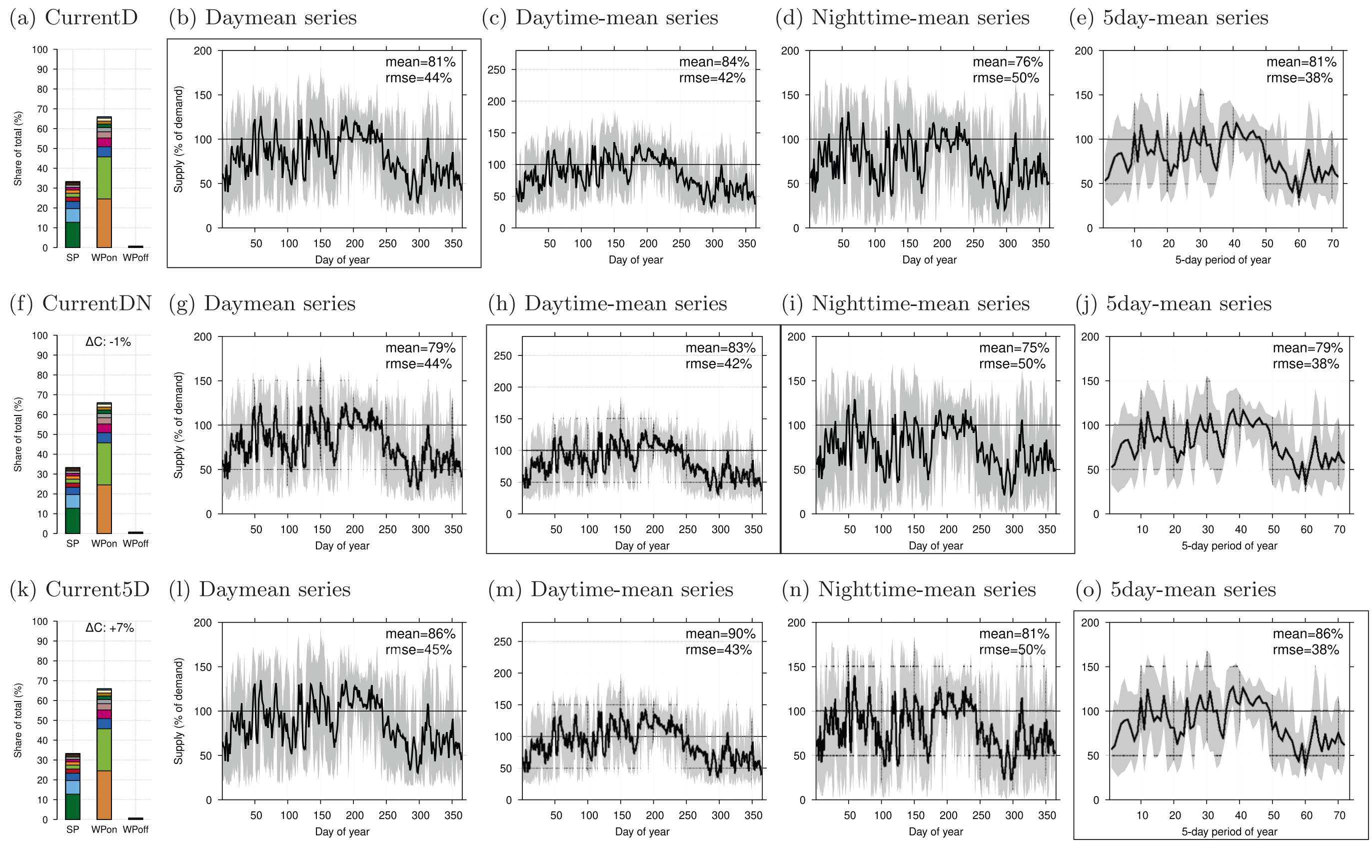

Fig. 4. Current scenarios. Left hand side panels depict the shares of each technology (in % of the total, i.e. of the sum of the SP, WP onshore, and WP offshore capacities) in each of the regions identified in Fig. 3 (as indicated by the color) according to different deployment scenarios, those that maintain the current shares and spatial distribution of the facilities pursuing to minimize the dispatch between production and demand considering daily means (CurrentD, panel a), day- and nighttime means (CurrentDN, panel f), or 5-day means (Current5D, panel k), by modifying the total installed capacity of both technologies (C). Taking as reference the value of C in the CurrentD scenario, △C in the two other scenarios is indicated at the top of panels f and k, respectively. To the right, the resulting supply series at the various time-scales. All supply values are expressed as a percentage of daily demand records and referred to the left Y-axis. Mean annual cycles are depicted with thick lines. Shadows around them represent the minimum-to-maximum range of individual records. The top-right corner of each panel shows the mean production and the *rmse* between production and demand, both first computed in absolute values and then expressed as a percentage of the mean demand throughout the period. Framed panels (b, the pair h&i, and o) are those approached in each optimization exercise.

offshore share). Notably, the total capacity required by this optimal strategy is half that in the case of the OptimD and Optim5D scenarios, while still achieving comparable mean supply levels (85% in the OptimDN scenario, 96% in the OptimD). More importantly, nighttime mean supply increases significantly from 16% (OptimD) to 69% (OptimDN). In terms of stability, rmse increases from 21% to 34% at the daily mean time-scale but decreases substantially at shorter time scales: from 65% to 31% at daytime, and from 85% to 46% at nighttime (Fig. 5 b-d *vs*. Fig. 5 g-i).

Compared to the Current scenario, all these optimal strategies offer clear advantages. The instability of the production in following the demand, as measured by rmse, is reduced to half in the OptimD and Optim5D scenarios, with mean production values close to 100%, representing increases of about 15, and 10 percentage points, respectively, compared to their analogous Current scenarios. The improvements achieved with the OptimDN strategy are more modest, with rmse reductions of 5 to 10 percentage points. Note that I_{tot} was optimized in the Current scenarios without imposing any restrictions on total renewable penetration. Therefore, the shortcomings of the current deployment strategy, compared to the optimal ones, are not due to lower I_{tot} values, since increasing them would not have resulted in better results (at least, in terms of rmse).

The role of shares vs. Spatial distribution

The optimal scenarios (Fig. 5, left panels) substantially differ from the Current ones (Fig. 4, left panels) in terms of both the total penetration and share of each energy, and the spatial distribution of the facilities. To disentangle the role of each factor, particularly the importance of the spatial distribution of facilities, we created the Base scenarios. These scenarios maintain the same total penetration and share of each energy as in the Optimal ones, but redistribute the facilities using a non-optimized criterion: for each energy, the same amount of installed capacity per grid cell (Fig. 6, left panels). This allocation strategy is not suboptimal, as it still permits taking advantage of the spatio-temporal complementarity of the resources by covering all regions [38], but it does not fully leverage it in an *ad hoc* manner.

Compared to the optimized solutions, the Base scenarios yield mean production values approximately 10 percentage points higher, but rmse values are 5 to 10 percentage points larger (Fig. 6b,h,i,o *vs*. 5b,h,i,o). This indicates that during the optimization process, high-productivity regions can be penalized to prioritize and exploit complementarity between regions and energy sources, emphasizing quality rather than just quantity [39]. Consequently, regions that may not rank highest in terms of mean productivity gain relevance due to their potential to complement others and enhance production stability.

Therefore, the spatial distribution of the facilities plays a key role in enhancing the stability and reliability of the production system.

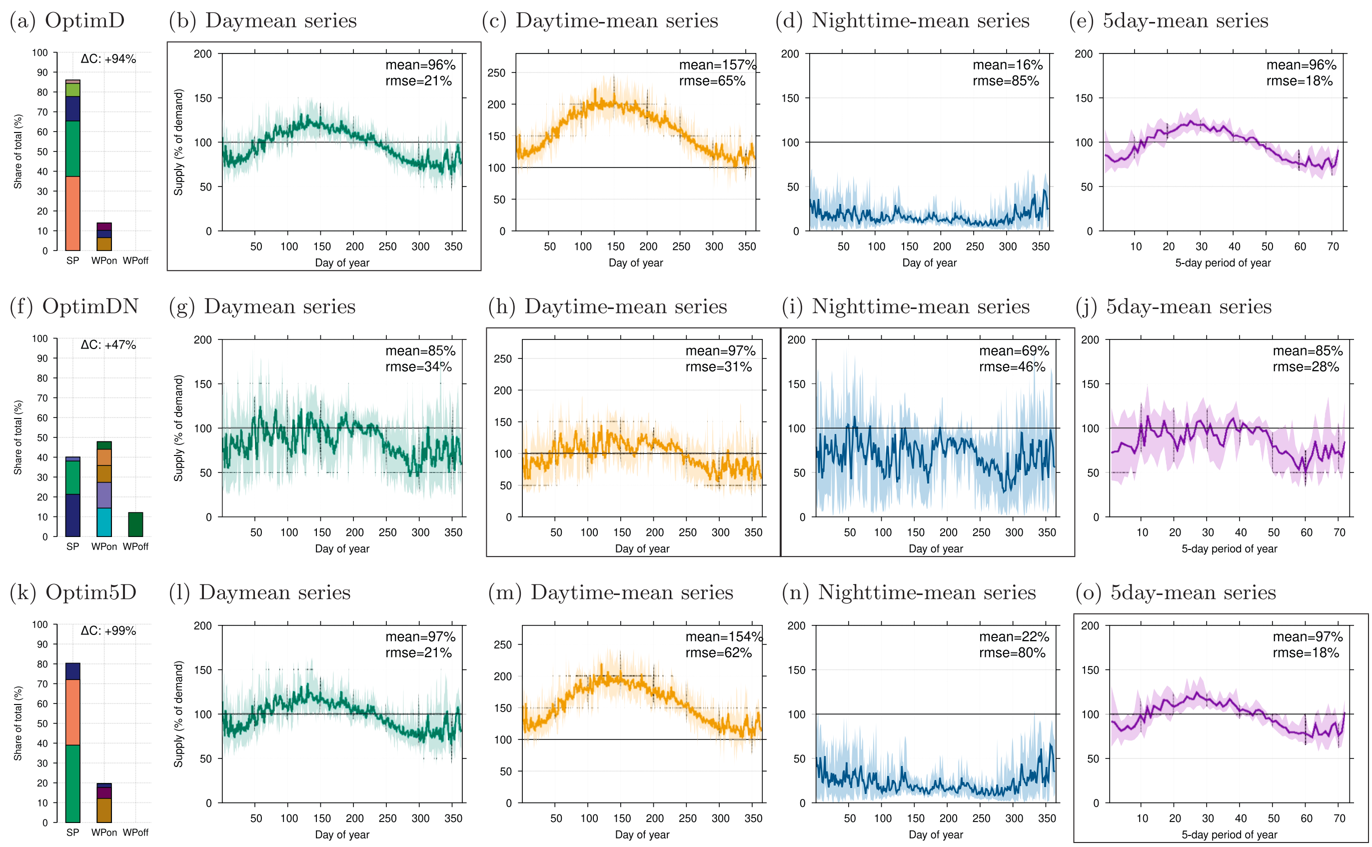

Fig. 5. Optimized scenarios. Left hand side panels depict the shares of each technology (in % of the total, i.e. of the sum of the SP, WP onshore, and WP offshore capacities) in each of the regions identified in Fig. 3 (as indicated by the color) according to different optimized deployment scenarios, those pursuing to minimize the dispatch between production and demand considering daily means (OptimD, panel a), day- and nighttime means (OptimDN, panel f), or 5-day means (Optim5D, panel k), by modifying the total installed capacity of both technologies (C), their shares and the spatial distribution of the facilities. Taking as reference the value of C in the CurrentD scenario, △C in these optimized scenarios is indicated at the top of panels a, f, and k, respectively. To the right, the resulting supply series at the various time-scales, as in Fig. 4. Framed panels (b, the pair h&i, and o) are those approached in each optimization exercise.

Compared to the Current scenario, improvements in rmse at the daytime and nighttime daily mean time scales are achieved only in the Optim scenario (Fig. 5h,i *vs.* 4 h,i), whereas the Base one provides similar results (Fig. 6h,i *vs.* 4 h,i). From there, it could seem that the penetration level of each technology plays only a marginal role, but it is certainly erroneous. CurrentDN (Fig. 4f), OptimDN (Fig. 5f), and BaseDN (Fig. 6f) scenarios are not very different in terms of SP *vs.* WP shares (33 *vs.* 66% in the CurrentDN, 40 *vs.* 60% in the other two), which prevents drawing conclusions about the role of energy shares. This result just highlights the importance of the spatial distribution of the facilities at that time-scale, but it does not mean a negligible role of the relative shares of each energy source. A balanced contribution of both factors emerges at the daily and 5-day mean time-scale (Fig. 4b,o, 5b,o, and 6b,o): half of the reduction in rmse achieved with the optimized solutions (compared to the Current ones) is also obtained with the Base scenarios, making it attributable to the relative shares of each energy, while the remaining half is only achieved with the Optim scenarios, indicating that it stems from the optimal spatial allocation of production units.

The role of urban areas

Current local regulations mandate that at least 7.5% of available rooftop area be covered with PV panels. This section aims to illustrate the potential urban contribution within the optimized scenarios previously described by considering three coverage thresholds: 7.5, 15, and 30%. For that, Fig. 7 shows the allocated SP capacity and the corresponding mean SP production across regions for selected scenarios (those labeled as DN, left panels), along with the urban area fraction and the mean SP production from urban areas assuming that as much as possible of the allocated SP capacity is installed on rooftops following the predefined coverage thresholds (right panels). Supplementary Figs. S2 and S3 show the results for the scenarios labeled as D and 5D (very similar conclusions are drawn regardless of the time-scale considered).

It should be noted that the Optim scenarios were generated without considering the restriction imposed by recent regulations regarding PV coverage on rooftops. As a result, these scenarios concentrate most of the SP capacity in a few regions (Fig. 7c and, e.g., S2c). To a lesser extent and for a different reason (rooftop regulation is recent and has no retroactive effect), a similar pattern is observed in the Current scenario (Fig. 7a). Consequently, the potential urban contribution is strongly influenced by the urban area fraction of these specific regions (Fig. 7b, d and S2b,d). For instance, both the OptimD and OptimDN scenarios allocate significant SP capacity to region #12, with approximately 15% and 50% of the total SP capacity in each scenario, respectively. However, this region, located in the northeasternmost corner of the domain, has an almost negligible urban area fraction (0.03%), making the potential contribution of urban rooftops nearly null. In contrast, region #14, situated on the northern coast of central Gran Canaria Island, which also hosts a substantial share of SP capacity in both scenarios (around 30% in OptimD and 40% in OptimDN), has an urban area fraction of 3%, which significantly enhances its contribution. If 7.5% of its rooftops were covered with PV panels, rooftop SP production would account for 4% of the regional SP production in the OptimD scenario and 9% in OptimDN; at 30% coverage, these figures rise to 17% and 37%, respectively. However, these relative contributions are also influenced

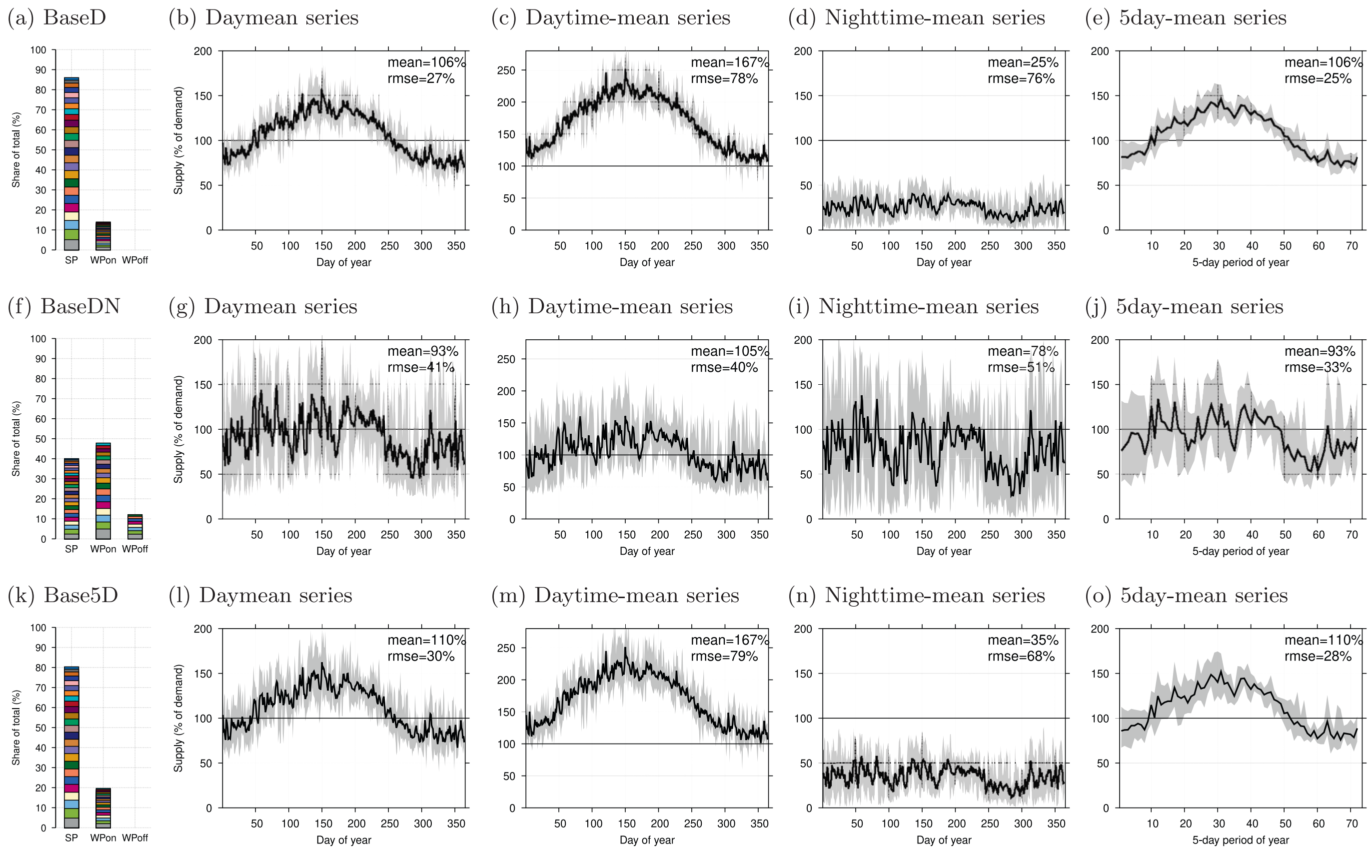

Fig. 6. Base scenarios. As Fig. 5 for the corresponding Base scenarios.

by the total SP capacity assigned to each region (and, therefore, its expected production), which varies across scenarios. In this sense, the urban role can appear amplified in regions where little SP capacity is allocated, even if these regions have few urban areas. This occurs, for instance, in region #23 (northwest of La Palma) under the OptimD scenario (Fig. S2c,d) and in region #15 (central part of Gran Canaria) under the OptimDN scenario (Fig. 7c,d). This interplay between urban area fraction and SP allocation complicates direct comparisons, making it challenging to draw clear conclusions.

The Base scenario distributes SP production units uniformly across regions and grid cells (Fig. 7e), providing a more reliable picture of the maximum potential of urban areas for contributing to renewable energy production (Fig. 7f). In this assessment, rooftop PV production represents 15–40% of total SP generation at 7.5% coverage, increasing to 55–100% at 30% coverage, in regions where urban areas exceed 1% of total land. This highlights the significant role that urban areas can play in renewable energy production when properly integrated into deployment strategies. Accomplishing this goal, the OptimUrban scenarios were generated. These, performing as good as the Optim scenarios (Fig. S4), leverage the role of urban areas, whose contribution, with 30% of rooftop PV coverage, uniformly increases up to 100% in most regions, 50% with 15% coverage, and 25% with 7.5% coverage (Fig. 7g,h, S2g,h, and S3g,h).

Conclusions and discussion

Without other than an explorative, mainly academic purpose, this research incorporates some real-world information (e.g., electricity demand records, practicable areas) in the first CLIMAX application beyond Jerez et al. [15], with the focus on a small, isolated domain. The results amply prove the potential of this framework to support strategic planning for renewable energy deployment. Although further research should, however, consistently investigate how these optimization principles hold under different climatic conditions[40–42], time-scales[8,9], grid constraints[43,44], and economic considerations[2,45], this study provides four key general insights. First, significant benefits can be achieved through the smart deployment of renewable energy units, enabling wind and solar power, as a combined system, to behave more like firm energy sources and better meet demand. In our case study, optimized strategies reduced the mismatch between production and demand by up to 20 percentage points compared to current deployment patterns. Second, optimizing both the relative shares of each technology and the spatial distribution of generation facilities is equally important in attaining these improvements: roughly half of the gains were attributable to adjusting the wind-to-solar ratio, and the other half to enhancing spatial complementarity. Third, regions with only moderate renewable productivity can play a crucial role in enhancing the stability of the overall system, challenging conventional planning strategies that focus predominantly on maximizing generation in high-yield locations. Finally, this study reinforces the strategic value of integrating ambitious urban targets into deployment plans: under a 30% rooftop PV coverage assumption, the CLIMAX solution showed system performance comparable to the fully optimized case without urban constraints. These findings are consistent with the literature, yet offer novel insights as discussed below.

Previous works have extensively explored the optimization of variable renewable energy deployment to address supply–demand balancing and improve energy system reliability. Many of these studies focus on a single technology[7,46,47], neglecting the advantage that wind–solar complementarity could offer, or explore it at a very local scale, delivering information relevant for individual hybrid systems (;[48,49]. Others focus on maximizing capacity factors, favoring the deployment of wind and solar power units in the most productive areas[14]. Yet, other studies address the optimization of wind–solar ratios to enhance

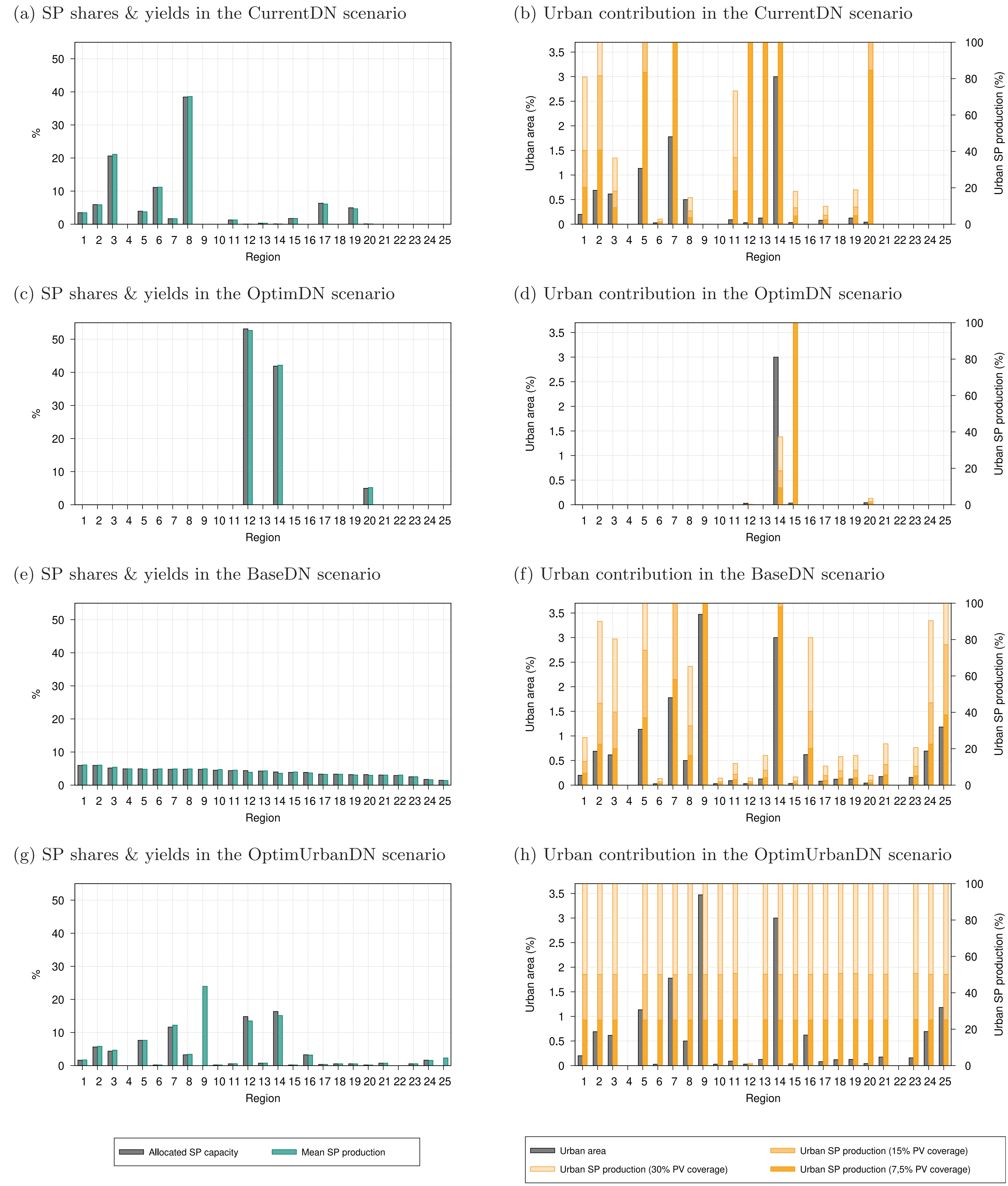

Fig. 7. Urban role. Left panels show the percentage of allocated solar power capacity (gray) and mean solar power production (green) in each region (% of total solar capacity and production, respectively) in different deployment scenarios (CurrentDN in the first row, OptimDN in the second, BaseDN in the third, and OptimUrbanDN in the fourth). Right panels provide the percentage of urban area in each region (gray, left y-axis, % of the total area of each region) and, for the same scenarios, the percentage of solar power production from urban areas (yellow, right y-axis, % of the mean solar production from each region) considering different levels of rooftop PV penetration (7,5%, 15% ans 30% of the urban area with solar panels).

large-scale system stability and demand matching[50,51], with some of them also accounting for optimized spatial allocation strategies[52–55]. Most of these studies, however, use administrative borders to define regional/national targets[52,54]for country- or continent-wide strategies (in which, sometimes, balancing across time zones plays a central role), which masks the resource complementarity potential within such borders.

This study provides new insights by disentangling the effects of spatial distribution from those of the technology mix in a small, isolated, yet highly variable regional context. For that, we followed the steps outlined by the CLIMAX methodology, a novel approach that defines regional targets using boundaries derived from climatological similarity, thereby maximizing the potential of optimized solutions. We demonstrate that optimizing the spatial deployment of renewable units is as critical as optimizing the relative share of each technology for improving system stability. Our approach also shows that considering regions with moderate renewable resource productivity can enhance system-wide stability due to their complementary temporal generation patterns, complementing and reinforcing findings from earlier studies on resource complementarity elsewhere, and that urban areas can play a key role in paving the way for solar power massive deployments, extending previous findings to different spatial and regulatory contexts.

It is important to note that the results presented here assume ideal inter-island interconnection, disregarding transmission losses. While this simplification facilitates the application of the CLIMAX framework and the illustration of its optimization potential, it does not account for real-world dispatch constraints, curtailment risks, or storage requirements. In the case of the Canary Islands, an archipelago with currently limited physical interconnection, the assumption of a fully interconnected system represents an upper-bound scenario in terms of system-wide complementarity and balancing potential. Nonetheless, the qualitative conclusions of this work remain valid under more realistic transfer constraints: regions with complementary generation patterns would still contribute to stability at the island scale, and smart allocation of technologies would still improve demand matching. Future research should further extend this work by explicitly incorporating grid topology, transfer limits, and storage dynamics to evaluate the robustness of these strategies under more realistic operational settings.

Code and data availability.

The CLIMAX codes used in this study can be downloaded from https://doi.org/10.5281/zenodo.7854945. The WRF configuration files and preprocessing scripts are available from the authors upon reasonable request. The wrf-python package used for the vertical interpolation of the simulated wind speed is accesible through https://wrf-python.readthedocs.io (last accessed on June 20, 2025). The electricity demand records are publicly available from Red Eléctrica de España (www.ree.es, last accessed on June 20, 2025).

CRediT authorship contribution statement

Sonia Jerez: Writing – original draft, Supervision, Software, Project administration, Methodology, Investigation, Funding acquisition, Formal analysis, Data curation, Conceptualization. **Judit Carrillo:** Writing – review & editing, Methodology, Formal analysis, Data curation. **Albano González:** Writing – review & editing, Resources, Methodology, Funding acquisition, Formal analysis, Data curation, Conceptualization. **Juan Pedro Díaz:** Writing – review & editing, Resources, Funding acquisition, Data curation, Conceptualization. **Francisco Javier Expósito:** Writing – review & editing, Resources, Data curation, Conceptualization. **Juan Carlos Pérez Darias:** Writing – review & editing, Resources, Data curation, Conceptualization.

Declaration of competing interest

The authors declare that they have no known competing financial interests or personal relationships that could have appeared to influence the work reported in this paper.

Acknowledgments

This study was supported by the Spanish Ministry of Science, Innovation, and Universities and the Agencia Estatal de Investigación (MCIN/AEI), and the European Union NextGenerationEU/PRTR, through the Grant Agreements TED2021-131074B-I00 and RYC2020-029993-I, and by the PLANCLIMAC2 Project (1/MAC/2/2.4/0006) financed through the European Union's INTERREG MAC 2021–2027 Program. The authors acknowledge the WCRP-CORDEX Flagship Pilot Study (FPS) on Macaronesian Archipelagos: Convection-Permitting Projections Focused on Island Processes (FPS-I-Mac).

Authors' contributions

S. J. conceived the study, generated the scenarios, carried out the analysis, and wrote the paper. J. C., A. G., J. P. D., F. J. E., and J. C. P. D. performed the WRF simulation, collected and provided all the other data used in this study, revised the manuscript, and contributed to discuss the results and write the paper.

Appendix A. Supplementary data

Supplementary data to this article can be found online at https://doi.org/10.1016/j.seta.2026.104949.

Data availability

Data will be made available on request.

References

[1] IPCC, 2022: *Climate Change 2022: Mitigation of Climate Change. Contribution of Working Group III to the Sixth Assessment Report of the Intergovernmental Panel on Climate Change* [P.R. Shukla, J. Skea, R. Slade, A. Al Khourdajie, R. van Diemen, D. McCollum, M. Pathak, S. Some, P. Vyas, R. Fradera, M. Belkacemi, A. Hasija, G. Lisboa, S. Luz, J. Malley, (eds.)]. Cambridge University Press, Cambridge, UK and New York, NY, USA. https://doi.org/10.1017/9781009157926.

[2] Ah-Voun D, Chyong CK, Li C. Europe's energy security: from Russian dependence to renewable reliance. Energy Policy 2024;184:113856. https://doi.org/10.1016/j.enpol.2023.113856.

[3] Cataldi M, Espinosa N, Jerez S, Montávez JP, Da Silveira LHM, Dupont J, et al. Balancing cleaner energy and geopolitical interests in the complex transition of the European electricity mix: from Fukushima to the Ukraine war. Discover Energy 2024;4(1):2. https://doi.org/10.1007/s43937-024-00026-8.

[4] Qays MO, Ahmad I, Habibi D, Moses P. Long-term techno-economic analysis considering system strength and reliability shortfalls of electric vehicle-to-grid-systems installations integrated with renewable energy generators using hybrid GRU-classical optimization method. Sustainable Energy Technol Assess 2025;76:104294. https://doi.org/10.1016/j.seta.2025.104294.

[5] Irena. Renewable energy statistics 2024. Abu Dhabi: International Renewable Energy Agency; 2024.

[6] Tobin I, Greuell W, Jerez S, Ludwig F, Vautard R, van Vliet MT, et al. Vulnerabilities and resilience of European power generation to 1.5 C, 2 C and 3 C warming. Environ Res Lett 2018;13(4):044024. https://doi.org/10.1088/1748-9326/aab211.

[7] Grams CM, Beerli R, Pfenninger S, Staffell I, Wernli H. Balancing Europe's wind-power output through spatial deployment informed by weather regimes. Nat Clim Chang 2017;7(8):557–62. https://doi.org/10.1038/nclimate3338.

[8] Wohland J, Brayshaw D, Pfenninger S. Mitigating a century of European renewable variability with transmission and informed siting. Environ Res Lett 2021;16(6):064026. https://doi.org/10.1088/1748-9326/abff89.

[9] Jerez S, Tobin I, Turco M, Jiménez-Guerrero P, Vautard R, Montávez JP. Future changes, or lack thereof, in the temporal variability of the combined wind-plus-solar power production in Europe. Renew Energy 2019;139:251–60. https://doi.org/10.1016/j.renene.2019.02.06.

[10] Jerez S, Trigo RM. Time-scale and extent at which large-scale circulation modes determine the wind and solar potential in the Iberian Peninsula. Environ Res Lett 2013;8(4):044035. https://doi.org/10.1088/1748-9326/8/4/044035.

[11] Olauson J. ERA5: the new champion of wind power modelling? Renew Energy 2018;126:322–31. https://doi.org/10.1016/j.renene.2018.03.056.

[12] Zeng Z, Ziegler AD, Searchinger T, Yang L, Chen A, Ju K, et al. A reversal in global terrestrial stilling and its implications for wind energy production. Nat Clim Chang 2019;9(12):979–85. https://doi.org/10.1038/s41558-019-0622-6.

[13] Jerez S, Palacios-Peña L, Gutiérrez C, Jiménez-Guerrero P, López-Romero JM, Pravia-Sarabia E, et al. Sensitivity of surface solar radiation to aerosol–radiation and aerosol–cloud interactions over Europe in WRFv3. 6.1 climatic runs with fully interactive aerosols. Geosci Model Dev 2021;14(3):1533–51. https://doi.org/10.5194/gmd-14-1533-2021.

[14] Wang Y, Wang R, Tanaka K, Ciais P, Penuelas J, Balkanski Y, et al. Global spatiotemporal optimization of photovoltaic and wind power to achieve the Paris Agreement targets. Nat Commun 2025;16(1):2127. https://doi.org/10.1038/s41467-025-57292-w.

[15] Jerez S, Barriopedro D, García-López A, Lorente-Plazas R, Somoza AM, Turco M, et al. An Action-Oriented Approach to Make the Most of the Wind and Solar Power Complementarity. Earth's Future 2023;11(6):e2022EF003332. https://doi.org/10.1029/2022EF003332.

[16] Langer J, Lombardi F, Pfenninger S, Rahayu HP, Al Irsyad MI, Blok K. The role of inter-island transmission in full decarbonisation scenarios for Indonesia's power sector. Environ Res: Energy 2024;1(2):025006. https://doi.org/10.1088/2753-3751/ad53cb.

[17] Skamarock WC, Klemp JB, Dudhia J, Gill DO, Barker DM, Duda MG, et al. A description of the advanced research WRF version 3. NCAR technical note 2008; 475(125):10–5065. https://doi.org/10.5065/D68S4MVH.

[18] Hersbach H, Bell B, Berrisford P, Hirahara S, Horányi A, Muñoz-Sabater J, et al. The ERA5 global reanalysis. Q J R Meteorolog Soc 2020;146(730):1999–2049. https://doi.org/10.1002/qj.3803.

[19] Pérez JC, Díaz JP, González A, Expósito J, Rivera-López F, Taima D. Evaluation of WRF parameterizations for dynamical downscaling in the Canary Islands. J Clim 2014;27(14):5611–31. https://doi.org/10.1175/jcli-d-13-00458.1.

[20] Pérez JC, González A, Díaz JP, Expósito FJ, Felipe J. Climate change impact on future photovoltaic resource potential in an orographically complex archipelago, the Canary Islands. Renew Energy 2019;133:749–59. https://doi.org/10.1016/j.renene.2018.10.077.

[21] Expósito FJ, González A, Pérez JC, Díaz JP, Taima D. High-resolution future projections of temperature and precipitation in the Canary Islands. J Clim 2015;28 (19):7846–56. https://doi.org/10.1175/jcli-d-15-0030.1.

[22] González A, Pérez JC, Díaz JP, Expósito FJ. Future projections of wind resource in a mountainous archipelago, Canary Islands. Renew Energy 2017;104:120–8. https://doi.org/10.1016/j.renene.2016.12.021.

[23] Lim K-S-S, Hong S-Y. Development of an effective double-moment cloud microphysics scheme with prognostic cloud condensation nuclei (CCN) for weather and climate models. Mon Weather Rev 2010;138:1587–612. https://doi.org/10.1175/2009MWR2968.1.

[24] Hong S-Y, Noh Y, Dudhia J. A new vertical diffusion package with an explicit treatment of entrainment processes. Mon Weather Rev 2006;134:2318–41. https://doi.org/10.1175/MWR3199.1.

[25] Chen F, Dudhia J. Coupling an advanced land surface-hydrology model with the Penn State-NCAR MM5 modeling system. Part I: model implementation and sensitivity. Mon Weather Rev 2001;129:569–85. https://doi.org/10.1175/1520-0493(2001)129%3C0569:CAALSH%3E2.0.CO;2.

[26] Collins, W. D. et al. (2004) Description of the NCAR Community Atmosphere Model (CAM 3.0). https://doi.org/10.5065/D63N21CH.

[27] Kain JS. The Kain-Fritsch convective parameterization: an update. J Appl Meteorol 2004;43:170–81. https://doi.org/10.1175/1520-0450(2004)0430170:TKCPAU>2.0.CO;2.

[28] DGIEGC (2021a). Dirección General de Industria y Energía del Gobierno de Canarias, WMS Parques Eólicos de Canarias, 2021-02-25, https://catalogo.idecanarias.es/geonetwork/srv/metadata/spagrafcan_PARQUESEOLICOSWMS_20160101/formatters/xsl-view [dataset].

[29] DGIEGC (2021b). Dirección General de Industria y Energía del Gobierno de Canarias, WMS Parques Fotovoltaicos de Canarias, 2021-03-08, https://catalogo.idecanarias.es/geonetwork/srv/metadata/spagrafcan_FOTOVOLTAICOSWMS_20200313/formatters/xsl-view [dataset].

[30] MTERD (2020). Ministerio para la Transición Ecológica y el Reto Demográfico (Dirección General de Calidad y Evaluación Ambiental). Zonificación ambiental para la implantación de energías renovables: eólica y fotovoltaica. https://www.miteco.gob.es/es/calidad-y-evaluacion-ambiental/temas/evaluacion-ambiental/zonificacion_ambiental_energias_renovables.html .

[31] GRAFCAN (2008). Cartográfica de Canarias S.A. Gobierno de Canarias, 2008-05-26. http://catalogo.idecanarias.es/geonetwork/srv/metadata/spagrafcan_131MOS2002WMS_20160101 .

[32] Ward Jr JH. Hierarchical grouping to optimize an objective function. J Am Stat Assoc 1963;58(301):236–44. https://doi.org/10.1080/01621459.1963.10500845.

[33] Salvador S, Chan P. Learning states and rules for detecting anomalies in time series. Appl Intell 2005;23(3):241–55. https://doi.org/10.1007/s10489-005-4610-3.

[34] Thorndike RL. Who belongs in the family? Psychometrika 1953;18(4):267–76. https://doi.org/10.1007/BF02289263.

[35] Hartigan JA, Wong MA. Algorithm AS 136: a k-means clustering algorithm. J Roy Stat Soc: Ser C (Appl Stat) 1979;28(1):100–8. https://doi.org/10.2307/2346830.

[36] Lorente-Plazas R, Montávez JP, Jerez S, Gómez-Navarro JJ, Jiménez-Guerrero P, Jiménez PA. A 49 year hindcast of surface winds over the Iberian Peninsula. Int J Climatol 2015;35(10):3007–23. https://doi.org/10.1002/joc.4189.

[37] Tröndle T, Pfenninger S, Lilliestam J. Home-made or imported: on the possibility for renewable electricity autarky on all scales in Europe. Energ Strat Rev 2019;26: 100388. https://doi.org/10.1016/j.esr.2019.100388.

[38] Giddings J, Bloomfield H, James R, Blair M. The impact of future UK offshore wind farm distribution and climate change on generation performance and variability. Environ Res Lett 2024;19(6):064022. https://doi.org/10.1088/1748-9326/ad489b.

[39] Antonini EG, Ruggles TH, Farnham DJ, Caldeira K. The quantity-quality transition in the value of expanding wind and solar power generation. Iscience 2022;25(4). https://doi.org/10.1016/j.isci.2022.104140.

[40] Van Ruijven BJ, De Cian E, Sue Wing I. Amplification of future energy demand growth due to climate change. Nat Commun 2019;10(1):2762. https://doi.org/10.1038/s41467-019-10399-3.

[41] Delort Ylla J, Tantet A, Drobinski P. Impact of climate change on high wind and solar optimal mixes and system costs: the case of France. Adv Geosci 2025;65: 159–69. https://doi.org/10.5194/adgeo-65-159-2025.

[42] Lv F, Tang H. Assessing the impact of climate change on the optimal solar–wind hybrid power generation potential in China: a focus on stability and complementarity. Renew Sustain Energy Rev 2025;212:115429. https://doi.org/10.1016/j.rser.2025.115429.

[43] Boßmann T, Staffell I. The shape of future electricity demand: Exploring load curves in 2050s Germany and Britain. Environ Res Lett 2015;8(4):044035. https://doi.org/10.1088/1748-9326/8/4/044035.

[44] Qays MO, Ahmad I, Habibi D, Aziz A, Mahmoud T. System strength shortfall challenges for renewable energy-based power systems: a review. Renew Sustain Energy Rev 2023;183:113447. https://doi.org/10.1016/j.rser.2023.113447.

[45] Yousif M, Ai Q, Wattoo WA, Jiang Z, Hao R, Gao Y. Least cost combinations of solar power, wind power, and energy storage system for powering large-scale grid. J Power Sources 2019;412:710–6. https://doi.org/10.1016/j.jpowsour.2018.11.084.

[46] Gutiérrez C, Gaertner MÁ, Perpiñán O, Gallardo C, Sánchez E. A multi-step scheme for spatial analysis of solar and photovoltaic production variability and complementarity. Sol Energy 2017;158:100–16. https://doi.org/10.1016/j.solener.2017.09.037.

[47] Prol JL, deLlano-Paz F, Calvo-Silvosa A, Pfenninger S, Staffell I. Spatial integration for firm and load-following wind generation. Environ Res Lett 2024;19(9):094026. https://doi.org/10.1088/1748-9326/ad5d7d.

[48] Schindler D, Behr HD, Jung C. On the spatiotemporal variability and potential of complementarity of wind and solar resources. Energy Convers. Manage. 2020;218: 113016. https://doi.org/10.1016/j.enconman.2020.113016.

[49] Couto A, Estanqueiro A. Assessment of wind and solar PV local complementarity for the hybridization of the wind power plants installed in Portugal. J Clean Prod 2021;319:128728. https://doi.org/10.1016/j.jclepro.2021.128728.

[50] Hou W, Zhang X, Wu M, Feng Y, Yang L. Integrating stability and complementarity to assess the accommodable generation potential of multiscale solar and wind resources: a case study in a resource-based area in China. Energy 2022;261: 125312. https://doi.org/10.1016/j.energy.2022.125312.

[51] Solomon AA, Child M, Caldera U, Breyer C. Exploiting wind–solar resource complementarity to reduce energy storage need. AIMS Energy 2020;8(5):749–70. https://doi.org/10.3934/energy.2020.5.749.

[52] Santos-Alamillos FJ, Brayshaw DJ, Methven J, Thomaidis NS, Ruiz-Arias JA, Pozo-Vázquez D. Exploring the meteorological potential for planning a high performance European electricity super-grid: optimal power capacity distribution among countries. Environ Res Lett 2017;12(11):114030. https://doi.org/10.1088/1748-9326/aa8f18.

[53] Costoya X, DeCastro M, Carvalho D, Arguilé-Pérez B, Gómez-Gesteira M. Combining offshore wind and solar photovoltaic energy to stabilize energy supply under climate change scenarios: a case study on the western Iberian Peninsula. Renew Sustain Energy Rev 2022;157:112037. https://doi.org/10.1016/j.rser.2021.112037.

[54] Prol JL, de Llano Paz F, Calvo-Silvosa A, Pfenninger S, Staffell I. Wind–solar technological, spatial and temporal complementarities in Europe: a portfolio approach. Energy 2024;292:130348. https://doi.org/10.1016/j.energy.2024.130348.

[55] Vázquez R, Cabos W, Nieto-Borge JC, Gutiérrez C. Complementarity of offshore energy resources on the spanish coasts: Wind, wave, and photovoltaic energy. Renew Energy 2024;224:120213. https://doi.org/10.1016/j.renene.2024.120213.